

Supplementary Information

Interface engineering of InP/ZnS core/shell quantum dots by the buffer monolayer for exceptional photocatalytic H₂ evolution

Rong-Jin Huang, Zhi-Kai Qin, Li-Lei Shen, Guangqiang Lv, Furong Tao,
Jingui Wang and Yu-Ji Gao*

Experimental Section

Characterization of photocatalysts

Powder X-ray diffraction (XRD) patterns were obtained by using Bruker D8 Focus (Bruker Corp, Billerica, MA, USA) with Cu-K α radiation. X-ray photoelectron spectroscopy (XPS) were recorded on an ESCALAB 250 spectrophotometer (Thermo Fisher Scientific Corp, Waltham, MA, USA) with Al-K α radiation. Elemental analysis data were obtained from Inductively Coupled Plasma Optical Emission Spectrometry (ICP-OES, Thermo Fisher ICP RQ, USA). FT-IR spectra were recorded on a Bruker Vertex 70 spectrometer. TEM and HRTEM images were obtained from JEM 2100 (JEOL Co. Ltd., Tokyo, Japan). UV-Vis absorption spectra were recorded on a Shimadzu UV-2600PC spectrophotometer (Shimadzu Corp, Kyoto, Japan). Photoluminescence (PL) spectra were obtained by Hitachi (model F-4600) spectrophotometer (Hitachi High-Tech Corp., Tokyo, Japan). The pH measurements were carried out by a Model Phs-3C meter (Mettler Toledo FE20, Mettler Toledo (Shanghai) Co. Ltd., Shanghai, China). The content of H₂ in the product was determined by gas chromatography (GC, GC-2014 Shimadzu, Shimadzu Corp., Kyoto, Japan) using N₂ as the carrier gas with a molecular sieve column (5Å; 30m×0.53mm) and a thermal conductivity detector. The photoelectrochemical measurement was carried out on an electrochemical workstation (CHI 660B, Chinstruments, Shanghai, China). High angle annular dark field (HAADF)-scanning transmission electron microscopy (STEM) images and energy-dispersive X-ray spectroscopy (EDS) maps were acquired using an aberration-corrected JEM-ARM300F operated at 80 kV. Femtosecond transient absorption (TA) spectroscopy was measured with pump pulse at 360 nm and probing with white light, the 360 nm pulse was produced by second-harmonic generation of the fundamental output of the Ti:sapphire regenerative amplifier (Coherent Legend Elite, 4 mJ, 25 fs, 1KHz).

Turnover numbering (TON) and apparent quantum efficiency (AQE) of catalysts

The TON of photocatalysts was estimated by the following equations (1):

$$\text{TON} = \frac{n(H_2)}{n(QDs)} \quad (1)$$

The apparent quantum efficiency (AQE) was measured under the monochromatic LED light sources ($\lambda = 460$ nm). The irradiation area was controlled as 4.5×1.3 cm². The accurate illumination power was 100 mW cm⁻². The AQE was calculated according to the following equation (2):

$$\text{AQE} [\%] = \frac{\text{Number of reacted electrons}}{\text{Number of incident photons}} \times 100\% = \frac{2 \times n(H_2) \times N_A}{S \times P \times t \times \frac{\lambda}{h \times C}} \quad (2)$$

Where, $n(H_2)$ is the amount of H₂ molecules (μmol) per hour; N_A is the Avogadro constant (6.022×10^{23} mol⁻¹); S is the irradiation area (cm²); P is the monochromatic light intensity (W cm⁻²); t is the light irradiation time (s); λ is the wavelength of the monochromatic light (nm); h is the Planck constant (6.626×10^{-34} J s); c is the speed of light (3×10^8 m s⁻¹).

Calculated the thickness of InP for anion exchange reaction

The InP QDs could be served as a uniform sphere with the diameter of ~ 2.86 nm. Therefore,

the radius of the InP QDs R_1 is 1.43 nm. So, the volume of InP QDs of V_1 can be calculated by the following equation:

$$V_1 = \frac{4}{3} \cdot \pi R_1^3$$

After the anion exchange reaction, about 50% of In-P bond is remained according to the XPS. So the remained volume of InP QDs of V_2 and radius of R_2 can be calculated by the following equation:

$$V_2 = \frac{1}{2} V_1 = \frac{4}{3} \cdot \pi R_2^3$$

The calculated $R_2 = 1.13$ nm, that is to say that the radius of InP core reduces by 0.30 nm after anion exchange, very close to the monolayer thickness of InP (0.332 nm) and ZnS (0.31 nm). Therefore, only about the outermost monolayer of InP is took place the anion exchange reaction.

Calculated the number of ZnS shell layers of CBS QDs:

First, for wurtzite structure of ZnS, the thicknesses of one ZnS ML is about 0.31 nm. When calculating the growth shell of each catalyst, taking CBS-100 as an example, the average size of the InP QDs increased from 2.86 nm to 4.02 nm after the coverage of ZnS, the thickness of ZnS shell d can be calculated by the following equation:

$$d = \frac{1}{2} \times (4.02 - 2.86) = 0.58 \text{ nm,}$$

The number of ZnS shell layers n can be calculated by the following equation:

$$n = \frac{\text{the thickness of shell}}{\text{the thicknesses of one ZnS ML}} = \frac{0.58}{0.31} = 1.87$$

Therefore, as for CBS-100 QDs, the increase of 0.58 nm shell thickness represents the 1.87 ZnS monolayer on average.

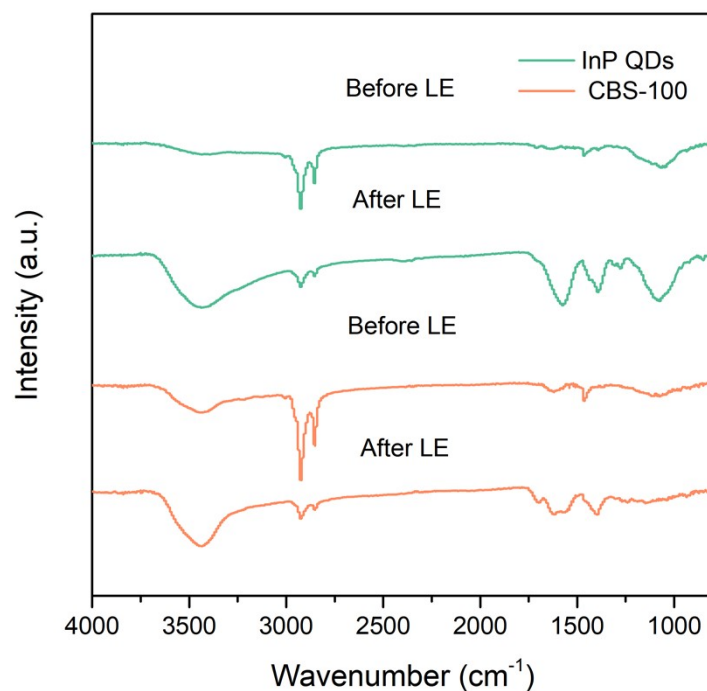


Fig. S1 FTIR spectra of InP and CBS-100 QDs before and after ligand exchange (LE). After ligand exchange, the intensity of C-H stretching vibration absorption peaks at 2924 cm^{-1} and 2850 cm^{-1} is significantly reduced, indicating that the ligand structure on the surface of the quantum dot has changed, and the long-chain oleylamine ligand on the surface of the original quantum dot has been replaced by MPA. No S-H characteristic peak was observed at 2370 cm^{-1} , which may be due to the fact that the MPA ligand was connected to the surface of the quantum dot through the thiol group. In addition, the absorption peaks at 1572 cm^{-1} and 1387 cm^{-1} may be attributed to the vibration absorption peaks of carboxyl groups.^{1,2}

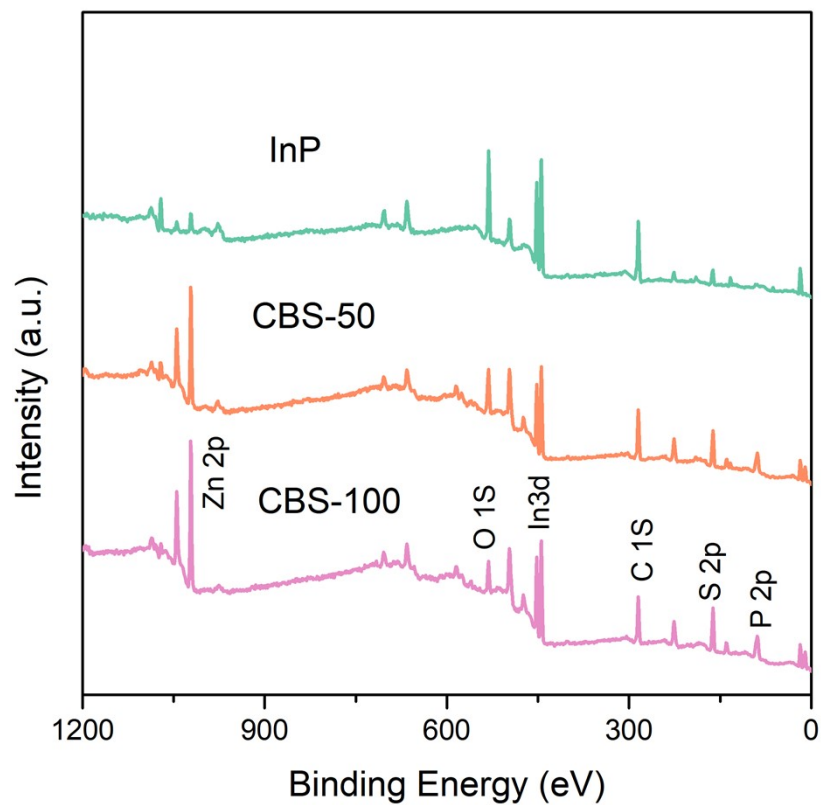


Fig. S2 The XPS survey spectra of InP, CBS-50 and CBS-100 QDs, respectively.

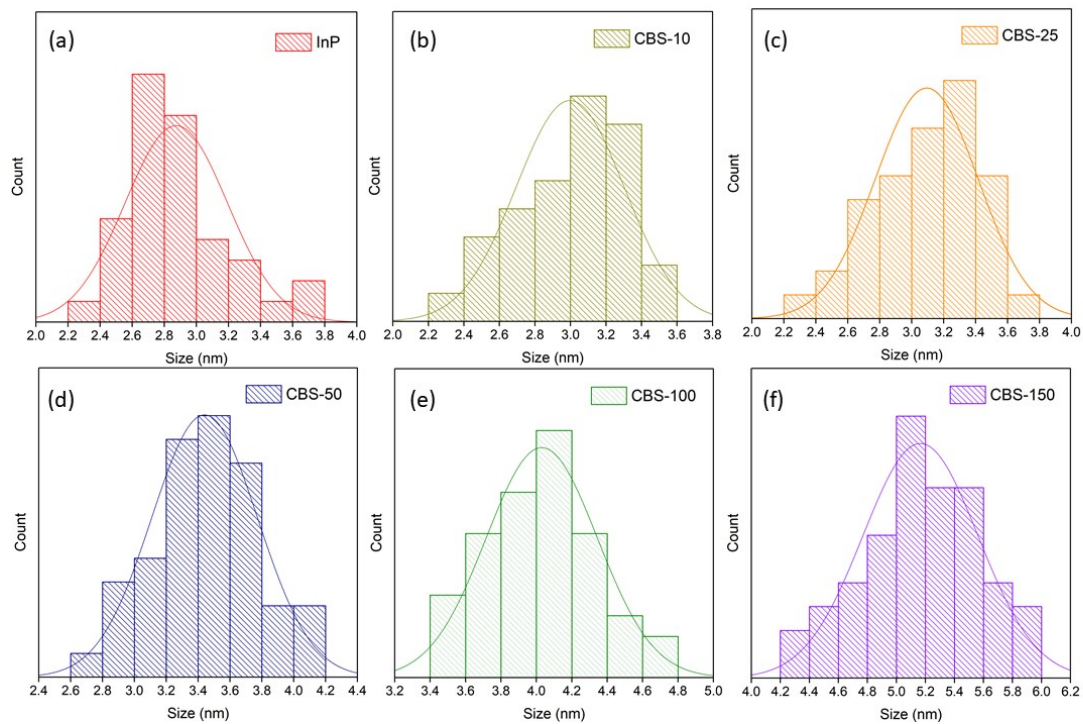


Fig. S3 Statistical analysis of the size distribution of QDs from TEM images. (a) InP QDs; (b) CBS-10; (c) CBS-25; (d) CBS-50; (e) CBS-100; (f) CBS-150.

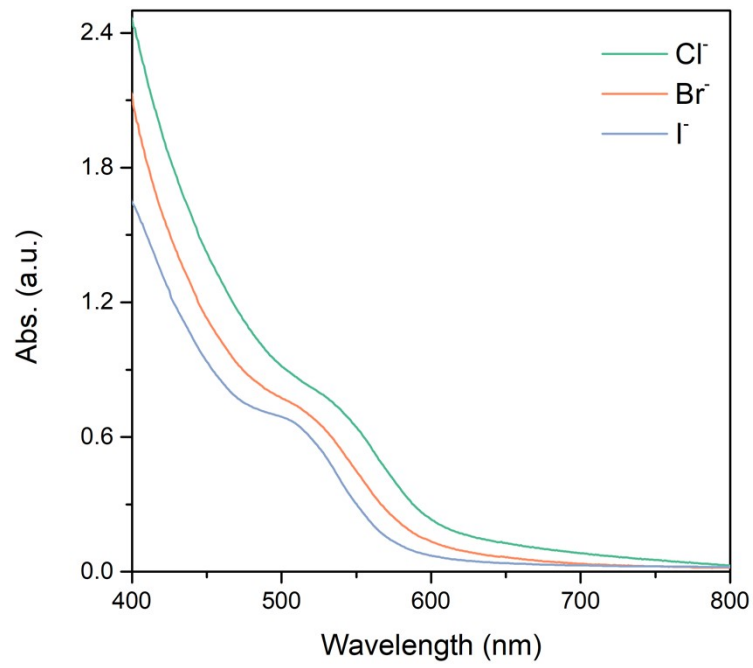


Fig. S4 UV-vis absorption spectra of InP QDs prepared by indium/zinc chloride, indium/zinc iodide and indium/zinc bromide. The red-shift of the absorption peaks for InP QDs prepared by indium/zinc chloride implies their larger size.

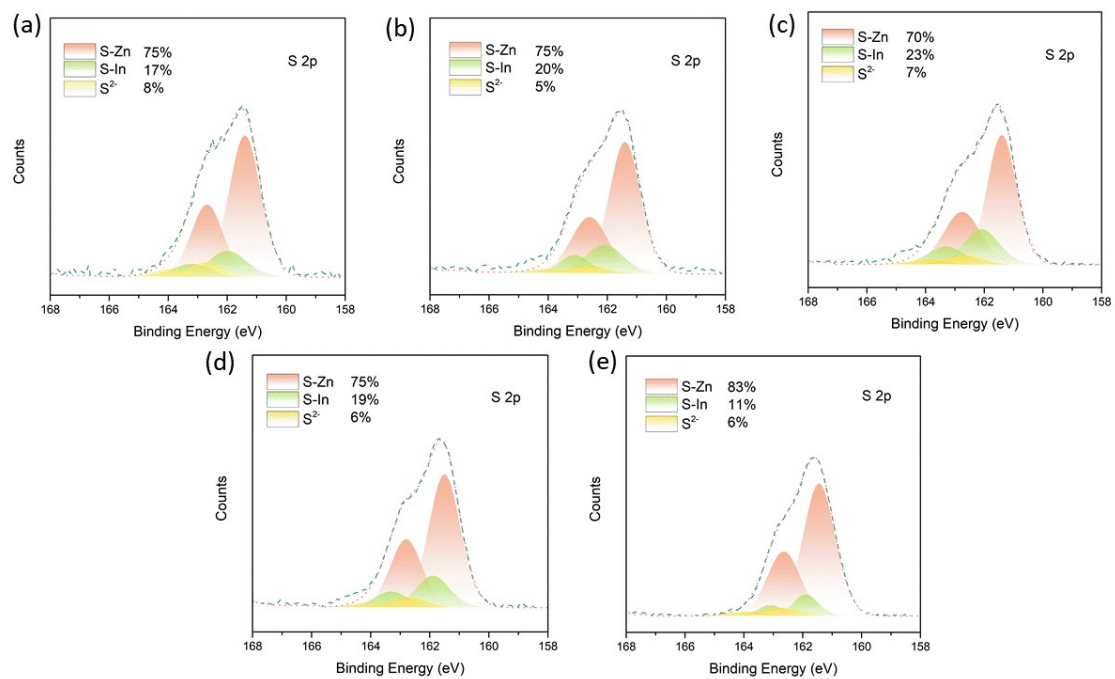


Fig. S5. High-resolution XPS analysis of S 2p spectra for (a) CBS-10, (b) CBS-25, (c) CBS-50, (d) CBS-100, (e) CBS-150.

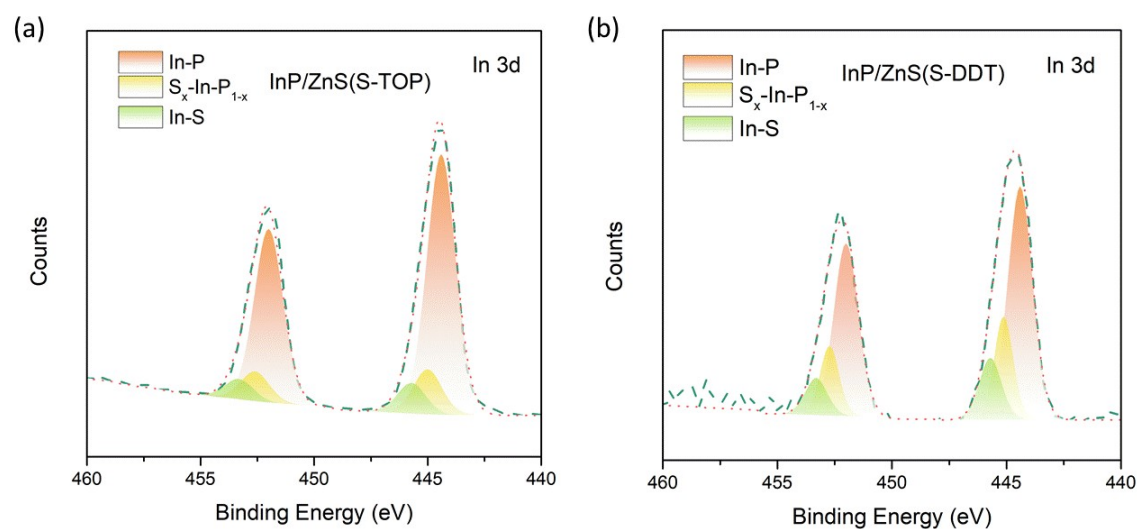


Fig. S6 High-resolution XPS analyses of In 3d spectra of InP/ZnS QDs synthesized by S-TOP (a) and S-DDT (b).

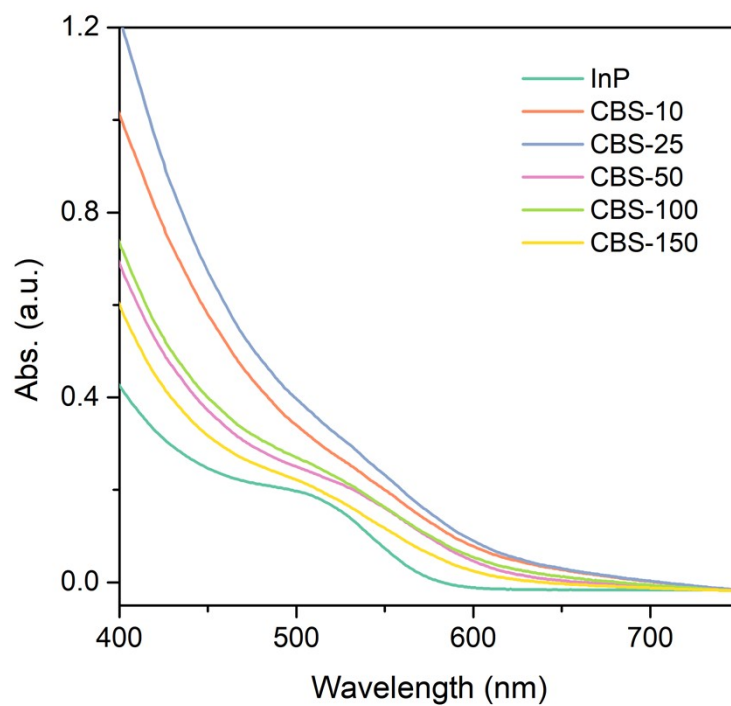


Fig. S7 UV-vis absorption spectra of InP and various CBS QDs.

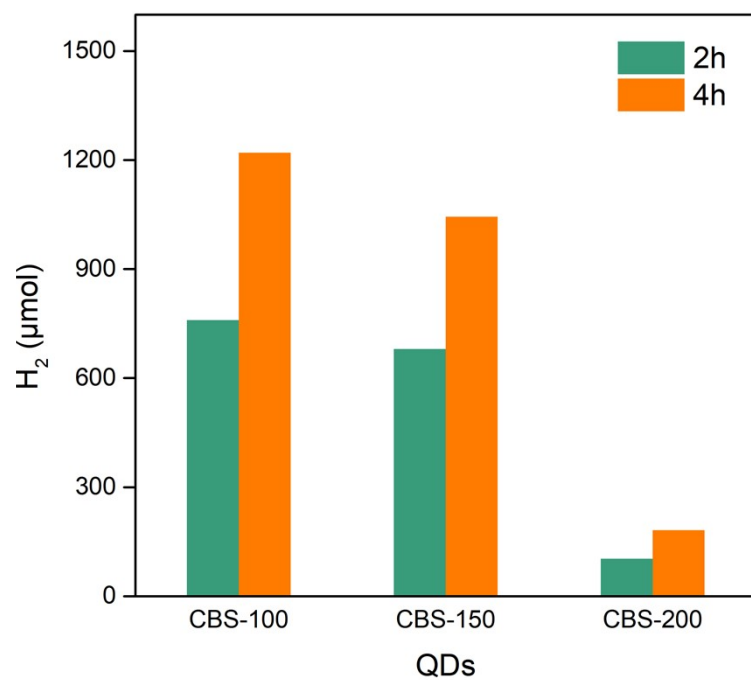


Fig. S8 Hydrogen evolution of CBS-100, CBS-150 and CBS-200 QDs under the identical concentration. The CBS-200 was synthesized in the same procedure with CBS-150 except for changing the concentration of S-ODE to 200 mM.

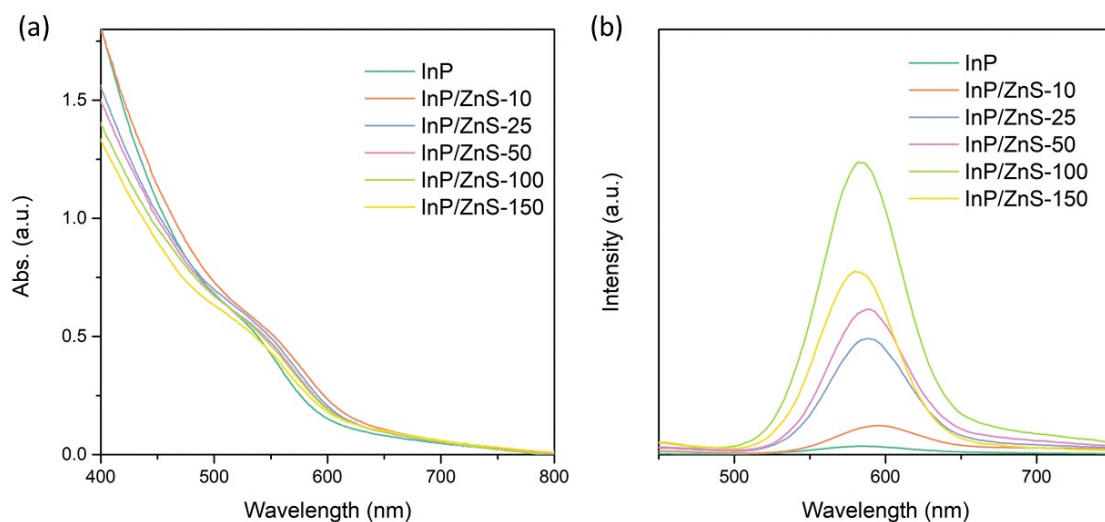


Fig. S9 UV-vis absorption spectra (a) and steady-state photoluminescent spectra (b) of InP/ZnS QDs (S-TOP).

The absorption peaks of InP/ZnS QDs (S-TOP) slightly blue-shift with the increased ZnS shell thickness. Which is due that the partial anion exchange results in the reduced size of InP core, just like the CBS QDs (Fig. S7). However, due to the limited anion exchange, the blue-shift is slight, which is also in line with that of the photoluminescent spectra. The spectroscopic characterizations indicate the preparation of InP/ZnS core/shell QDs without the significant anion exchange.

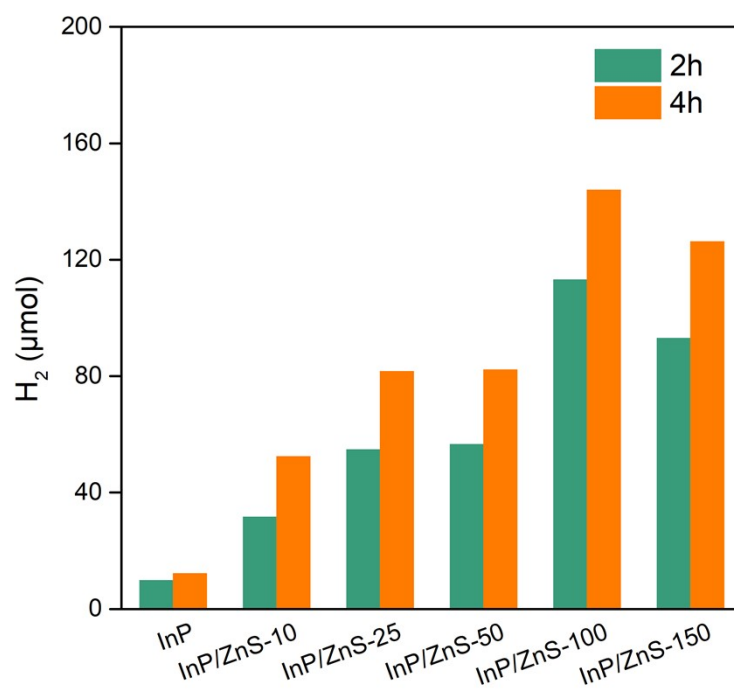


Fig. S10 Photocatalytic hydrogen evolution of InP and InP/ZnS QDs synthesized by S-TOP. Here, InP/ZnS-10, InP/ZnS-25, InP/ZnS-50, InP/ZnS-100 and InP/ZnS-150 indicates that the concentration of S-TOP used to prepare InP/ZnS QDs were 10 mM, 25 mM, 50 mM, 100 mM and 150 mM, respectively.

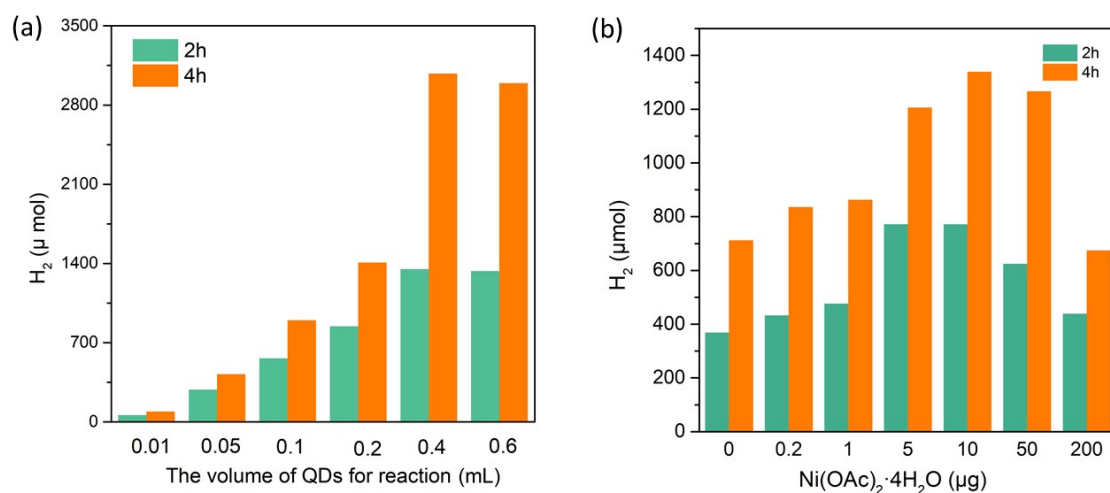


Fig. S11 Comparison of H₂ evolution of CBS-100 QDs under the (a) different volume of QDs for reaction; (b) different mass of Ni(CH₃COO)₂·4·H₂O, respectively. Conditions: (a) corresponding volume of CBS-100 QDs (67.8 μmol L⁻¹) with 6.7 μM Ni²⁺ in 6 mL of 0.34 M Na₂A (pH 4.5) were illuminated with 460 nm LEDs; (b) 2.26 μM CBS-100 QDs with different mass of Ni(OAc)₂·4H₂O in 6 mL of 0.34 M Na₂A (pH 4.5) were illuminated with 460 nm LEDs.

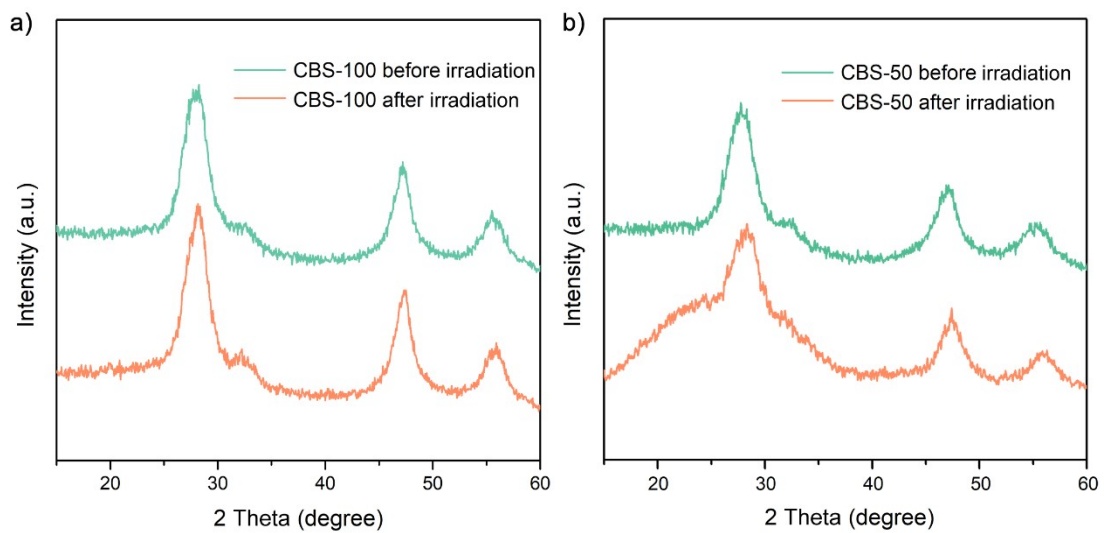


Fig. S12 The comparison of powder XRD patterns of CBS-100 QDs (a) and CBS-50 QDs (b) before and after irradiation.

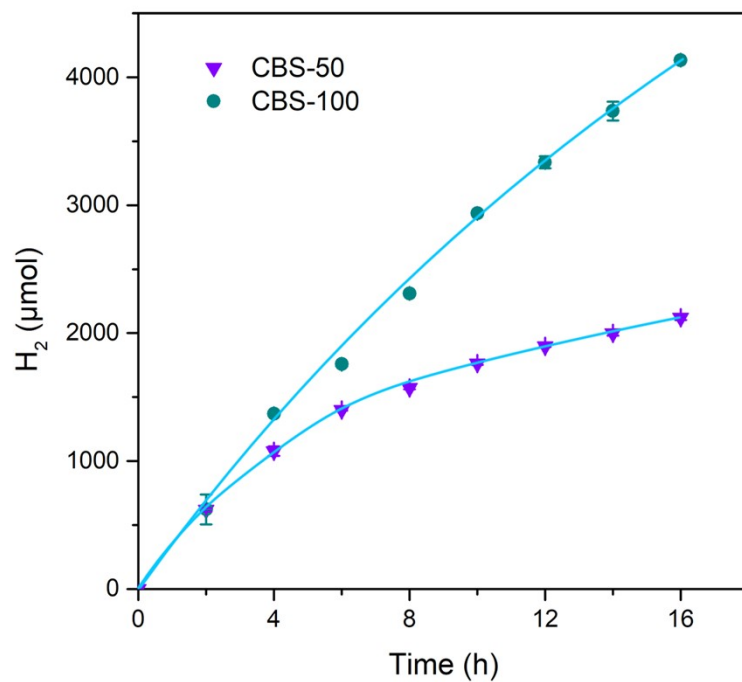


Fig. S13 The photocatalytic H₂ evolution comparison of CBS-50 and CBS-100 QDs with identical concentration under the optimal conditions. Error bars are estimated based on the standard deviation according to multiple independent experiments.

Table S1. Comparison of photocatalytic H₂ evolution with reported colloidal nanocrystals (NCs) - based systems.

Photocatalyst	Co-catalyst	Light Source	Donor	Rate of H ₂ Evolution	TON	Time (h)	Refer
InP/ZnS-S QDs	Ni ²⁺	453 nm	H ₂ A	45 mmol g ⁻¹ h ⁻¹	128000 vs. QDs	65.4	3
InP/Cu:ZnS QDs	Ni ²⁺	>400 nm	AA	----	403800 vs. QDs	40	4
InP QDs (Zn ²⁺ modified)	None	460 nm	Na ₂ SO ₃	7.6 mmol g ⁻¹ h ⁻¹	----	10	5
CdSe/CdS QDs	Pt NPs	450 nm	TEA	13.9 μmol h ⁻¹	1.4 × 10 ⁷ vs. Pt NPs	2	6
CdS/CdO _x QDs	None	AM 1.5G	Cellulose	4.4 mmol g ⁻¹ h ⁻¹	93030 vs. QDs	144	7
CdSe QDs	[FeFe]-H ₂ ase	>400 nm	H ₂ A	----	3 206 vs. QDs	80	8
CdS QDs	None	≥ 400 nm	N ₂ H ₄ ·H ₂ O	33 mmol g ⁻¹ h ⁻¹	14.16 vs. QDs	4	9
CdS QDs	Co ²⁺	>420 nm	Na ₂ SO ₃	25.41 mmol g ⁻¹ h ⁻¹ [a]	12160 vs. QDs	4	10
CdS QDs	Cobaloxime	>420 nm	TEOA	2.3 mmol g ⁻¹ h ⁻¹ [a]	171 vs. catalyst	15	11
CdSe QDs	Ni-DHLA	520 nm	H ₂ A	----	1 200 000 vs. QDs	360	12
CdTe QDs	Co ²⁺	>400 nm	H ₂ A	25 μmol h ⁻¹ mg ⁻¹	219 100 vs. QDs	70	13
CdSe QDs	Ni ²⁺	>400 nm	IPA	----	15 340 vs. QDs	20	14
CdSe/CdS QDs	Pt nanoparticle	450 nm	TEA	522.88 μmol h ⁻¹ [a]	1.6×10 ⁷ vs. Pt nanoparticle	8	15
ZnS modified CdSe QDs	None	450 nm	H ₂ A	306.3 ± 21.1 μmol mg ⁻¹ h ⁻¹	440 000 vs. QDs	40	2
CdSe QDs	ZnSe	>400 nm	H ₂ A	~30 000 μmol h ⁻¹ g ⁻¹	~5000 vs. QDs	12	16
InP/InPS/ZnS CBS QDs	Ni ²⁺	460 nm	H ₂ A	102.04 μmol mg ⁻¹ h ⁻¹	304867 vs. QDs	16	This work

[a]: The data is calculated according to the relevant data in the article.

Table S2 Kinetic analysis of emission decay for InP and CBS QDs.

Simple	τ_1 (ns)	τ_2 (ns)	A_1	A_2	τ_{ave}(ns)
InP	0.80	24.93	77.2	22.8	6.30
CBS-10	3.22	20.32	27.45	72.55	15.63
CBS-25	10.39	61.28	48.27	51.73	36.72
CBS-50	15.32	65.48	50.84	49.16	39.98
CBS-100	14.73	61.98	47.87	52.13	39.36
CBS-150	22.40	74.65	50.91	49.09	48.05

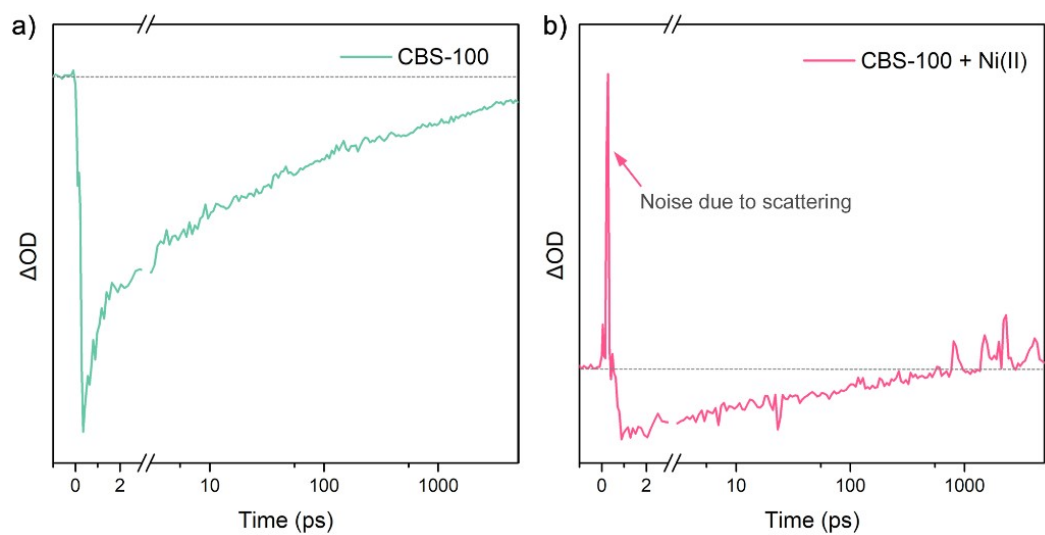


Fig. S14 The femtosecond transient absorption kinetics of CBS-100 QDs before (a) and after (b) adding the cocatalysts of Ni²⁺ at 510 nm.

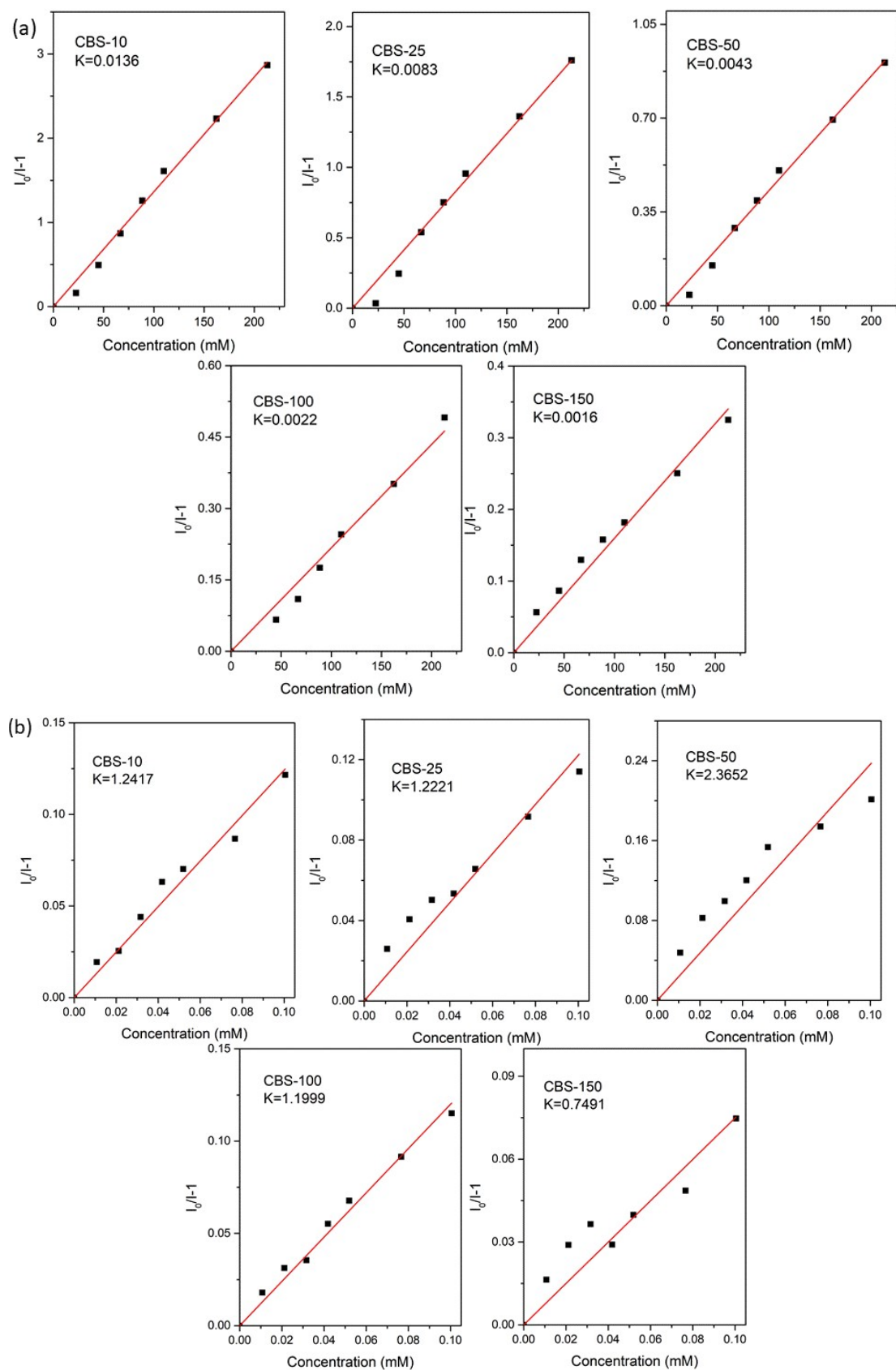


Fig. S15 Stern-Volmer plots of CBS QDs derived from $[I_0/I-1]$ vs. the concentration of H_2A (a) and Ni^{2+} (b), and the corresponding quenching constant (k) can be found in the figures.

Table S3 The quenching constants (k), photoluminescence lifetime (τ_0) and the corresponding electron transfer rates (k_{ET}) and hole transfer rates (k_{HT}) of the CBS QDs ($K_{ET/HT} = k/\tau_0$).

	CBS-10	CBS-25	CBS-50	CBS-100	CBS-150
k (mM ⁻¹)	1.24	1.22	2.37	1.20	0.75
τ_0 (ns)	15.62	36.71	39.98	39.36	48.05
k_{ET} ($\times 10^3$ M ⁻¹ s ⁻¹)	79.49	33.23	59.30	30.49	15.61

	CBS-10	CBS-25	CBS-50	CBS-100	CBS-150
k (mM ⁻¹)	0.014	0.0083	0.0043	0.0022	0.0016
τ_0 (ns)	15.62	36.71	39.98	39.36	48.05
k_{HT} ($\times 10^3$ M ⁻¹ s ⁻¹)	0.87	0.23	0.11	0.06	0.03

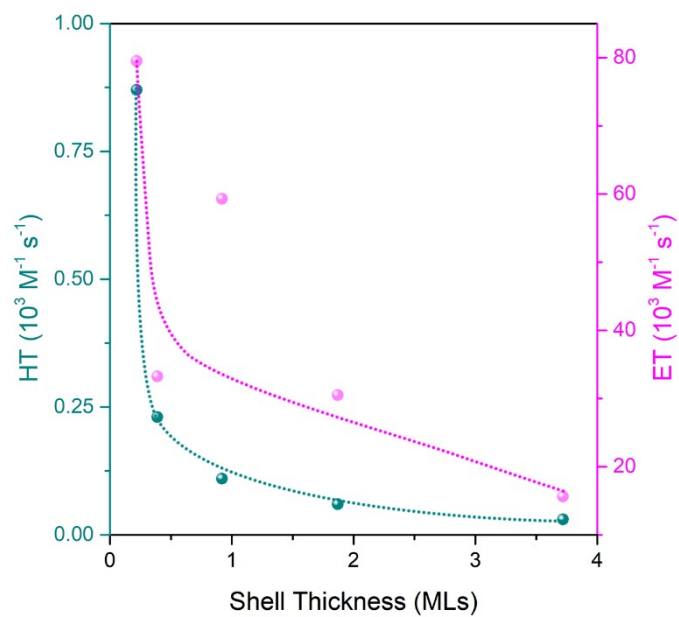


Fig. S16 Electron transfer (ET) and hole transfer (HT) rate variation of QDs/water interface with the increase of shell thickness.

References

1. P.-R. Chen, K.-Y. Lai, C.-W. Yeh and H.-S. Chen, *ACS Appl. Nano Mater.*, 2021, **4**, 3977-3988.
2. Y.-J. Gao, X.-B. Li, H.-L. Wu, S.-L. Meng, X.-B. Fan, M.-Y. Huang, Q. Guo, C.-H. Tung and L.-Z. Wu, *Adv. Funct. Mater.*, 2018, **28**, 1801769.
3. S. Yu, X.-B. Fan, X. Wang, J. Li, Q. Zhang, A. Xia, S. Wei, L.-Z. Wu, Y. Zhou and G. R. Patzke, *Nat. Commun.*, 2018, **9**, 4009.
4. J. Bang, S. Das, E.-J. Yu, K. Kim, H. Lim, S. Kim and J. W. Hong, *Nano Lett.*, 2020, **20**, 6263-6271.
5. S. Yu, Z. Xie, M. Ran, F. Wu, Y. Zhong, M. Dan and Y. Zhou, *J. Colloid Interface Sci.*, 2020, **573**, 71-77.
6. Y. Wang, X.-B. Li, H.-L. Wu, Y. Yang, Z. Liu, L.-P. Zhang, C.-H. Tung and L.-Z. Wu, *ACS Sustainable Chem. Eng.*, 2019, **7**, 7286-7293.
7. D. W. Wakerley, M. F. Kuehnel, K. L. Orchard, K. H. Ly, T. E. Rosser and E. Reisner, *Nat. Energy*, 2017, **2**, 17021.
8. C.-B. Li, Z.-J. Li, S. Yu, G.-X. Wang, F. Wang, Q.-Y. Meng, B. Chen, K. Feng, C.-H. Tung and L.-Z. Wu, *Energy Environ. Sci.*, 2013, **6**, 2597-2602.
9. M. K. Jana, U. Gupta and C. N. R. Rao, *Dalton Trans.*, 2016, **45**, 15137-15141.
10. C. M. Chang, K. L. Orchard, B. C. M. Martindale and E. Reisner, *J. Mater. Chem.A*, 2016, **4**, 2856-2862.
11. F. Wen, J. Yang, X. Zong, B. Ma, D. Wang and C. Li, *J. Catal.*, 2011, **281**, 318-324.
12. Z. Han, F. Qiu, R. Eisenberg, P. L. Holland and T. D. Krauss, *Science*, 2012, **338**, 1321-1324.
13. Z.-J. Li, X.-B. Li, J.-J. Wang, S. Yu, C.-B. Li, C.-H. Tung and L.-Z. Wu, *Energy Environ. Sci.*, 2013, **6**, 465-469.
14. Z.-J. Li, J.-J. Wang, X.-B. Li, X.-B. Fan, Q.-Y. Meng, K. Feng, B. Chen, C.-H. Tung and L.-Z. Wu, *Adv. Mater.*, 2013, **25**, 6613-6618.
15. X.-B. Li, Y.-J. Gao, Y. Wang, F. Zhan, X.-Y. Zhang, Q.-Y. Kong, N.-J. Zhao, Q. Guo, H.-L. Wu, Z.-J. Li, Y. Tao, J.-P. Zhang, B. Chen, C.-H. Tung and L.-Z. Wu, *J. Am. Chem. Soc.*, 2017, **139**, 4789-4796.
16. Y.-J. Gao, Y. Yang, X.-B. Li, H.-L. Wu, S.-L. Meng, Y. Wang, Q. Guo, M.-Y. Huang, C.-H. Tung and L.-Z. Wu, *Chem. Commun.*, 2018, **54**, 4858-4861.